Aalborg Universitet

A Low-Profile and Beam-Steerable Transmitarray Antenna

Design, Fabrication, and Measurement [Antenna Applications Corner]

Mei, Peng; Zhang, Shuai; Pedersen, Gert Frølund

A Low-Profile and Beam-Steerable Transmitarray Antenna: Design, Fabrication, and Measurement

Peng Mei, *Student Member, IEEE*, Shuai Zhang, *Senior Member, IEEE*, and Gert Frølund Pedersen, *Member, IEEE*

Abstract— **This paper describes the design, fabrication, and measurement of a low-profile and beam-steerable transmitarray (TA) antenna based on ray-folding principles. The proposed TA antenna consists of a planar feeding source, phase-shifting surfaces, and a metal plate as a reflector. The electromagnetic (EM) wave radiating from the planar feeding source would be reflected firstly by the metal plate, and then propagate through the phase-shifting surfaces to achieve a focused beam at broadside. In this configuration, the profile of the proposed TA antenna is decreased to half compared with a conventional TA antenna. To demonstrate the superiorities of the proposed TA antenna, the reflection coefficients, radiation patterns, and realized gains of three antennas, namely, the proposed TA antenna, a reflectarray (RA) antenna for reference, and a TA antenna for reference are simulated, compared, discussed, and measured. It is concluded that the proposed TA antenna has a comparable realized gain and lower profile. The simulated results reveal the proposed TA antenna has a realized gain of 24.8 dBi at 28 GHz with a profile of 20 mm ($1.87\lambda_0$ at 28 GHz), resulting in an aperture efficiency of 31.3 %, which are experimentally verified. The proposed TA antenna is also expanded to achieve beam steering. A prototype of a beam-steerable TA antenna with five beams is fabricated and measured, where main beams at ± 16º, ± 8º, 0º are observed with a gain variation of 2.4 dB and a broadside gain of 24.0 dBi corresponding to an aperture efficiency of 27 % at 27.2 GHz.**

Index Terms — **beam-steerable, low-profile, ray-folding principles, transmitarray antenna.**

I. INTRODUCTION

5G millimeter-wave has attracted many interests since they are good solutions to fulfil the communication requirements in the near future. 5G millimeter-wave can provide high-speed data rates, large channel capacities, etc., compared to the sub-6GHz bands in wireless communication applications [1], [2]. Antennas serving for transmitting and receiving electromagnetic (EM) waves are extremely important components in wireless systems. Compact size, high gain, and steerable beams are preferred for antennas in millimeter-wave bands to adapt the changeable environments and maintain high communication qualities [3].

There are some solutions to achieve high gain and beam steering [4]-[10]. The conventional one is a phased-array antenna, where every antenna element connects with a phase shifter. By manipulating the phase of each phase shifter individually, a two-dimensional beam steering is obtained. The phased-array antenna in the mm-wave bands, however, suffers from the high RF-component losses and the complicated beam-forming networks. Reconfigurable transmitarray (TA) or reflectarray (RA) antennas can also achieve beam steering by loading active RF components [11]-[14]. By controlling the DC voltage of varactor diodes, the transmission or reflection phase of each unit cell can be manipulated independently and continuously to achieve beam steering. However, the reconfigurable TA antennas are not suitable since controlling varactor diodes consumes too much power. Besides, it is difficult to access commercial mm-wave varactor diodes able to survive in large tempeture variations of -170 to 230 degrees Celsius for low earth orbit, and -250 to 300 degrees Celsius for other orbits.

Recently, passive TA and RA antennas are employed to achieve beam steering by switching among multiple feeding sources [15]-[19]. Each feeding source is responsible for one fixed beam at a specified direction. Unlike the phased-array and reconfigurable TA or RA antennas, the architectures of the passive TA and RA antennas with multiple feeding sources are simple, low-loss, and lightweight, without using any RF components. To decrease the profile of the beam-steerable TA or RA antennas, folded TA and RA antennas have emerged by introducing metal strips served as a polarizer to reflect the EM wave radiating from the feeding source firstly, and then propagate through the phase-shifting surfaces to achieve a focused beam in a specified direction [20]-[23]. In this configurable, the profile of a folded TA or RA antenna is decreased to half than that of a conventional TA or RA antenna. However, due to the polarization discrimination properties of a polarizer that only allowing a certain polarized EM wave passes through it, such folded RA and TA antennas are all single polarizations.

In this paper, we propose a low-profile TA antenna by using ray-folding principles. We first explain the mechanisms of the

proposed TA antenna, then we design a planar patch antenna serving as the feeding source, where a metal cavity is introduced to improve the radiation patterns of the feeding source. To demonstrate the superiorities of the proposed TA antenna, two referable antennas, namely, a RA antenna whose profile is the same as the proposed TA antenna, and a TA antenna whose profile is twice than the proposed TA antenna are also simulated and compared. The proposed TA antenna is also expanded to achieve beam-steerable abilities by using multiple feeding sources, the resolution of beam steering of the proposed beam-steerable TA antenna is also discussed. The proposed TA antenna, the RA antenna for reference, the TA antenna for reference, and the beam-steerable TA antenna with five beams are all fabricated, measured, and discussed finally.

Compared with the existing folded RA and TA antennas with fixed beam [20]-[23] and steerable beams [15]-[18], the proposed antenna has the following advantages:

- a lower profile (1.87 λ at 28 GHz) with a comparable aperture efficiency (31.3 %) is achieved;
- a metal plate is employed to replace the polarizer used in the existing folded TA and RA antennas, and the unit cells for phase-shifting surfaces implementations are highly symmetrical, the proposed TA antennas are therefore feasible for dual-polarized applications;
- a simpler design procedure, where only phase-shifting surfaces need to be synthesized. In contrast, a surface with polarization rotation and phase-shifting properties simultaneously is required for the existing folded TA and RA antennas;
- a beam-steerable TA antenna achieves ± 16º, ± 8º, 0º beam pointing directions and a broadside gain of 24.0 dBi corresponding to an aperture efficiency of 27 % is achieved, while still keeping the low profile of 1.87λ at 28 GHz.

II. LOW-PROFILE TRANSMITARRAY ANTENNA WITH A FIXED BEAM

The proposed low-profile TA antenna based on the ray-folding principles is described. Fig. 1 presents the schematic diagram of the proposed low-profile TA antenna. It consists of a metal plate served as a reflective surface, a feeding source, and phase-shifting surfaces. The feeding source and the phase-shifting surfaces are in the same aperture for an integrated design, while the metal plate is located below the TA phase-shifting surfaces. In this architecture, the electromagnetic wave radiating from the feeding source would be reflected by the metal plate firstly, and then propagate through the phase-shifting surfaces to achieve a focused beam in a specified direction. The extra propagation paths caused by the metal plate is expected to reduce the entire profile of the TA antenna to half compared to a conventional TA antenna. The profile of a RA or TA antenna is typically characterized by the ratio of focal-length-to-diameter. For the low-profile TA antenna shown in Fig. 1, the ration of focal-length-to-diameter is $F/2D$.
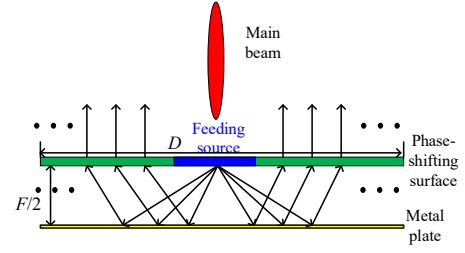

Fig. 1. The schematic diagram of the proposed low-profile TA antenna using ray-folding principles.
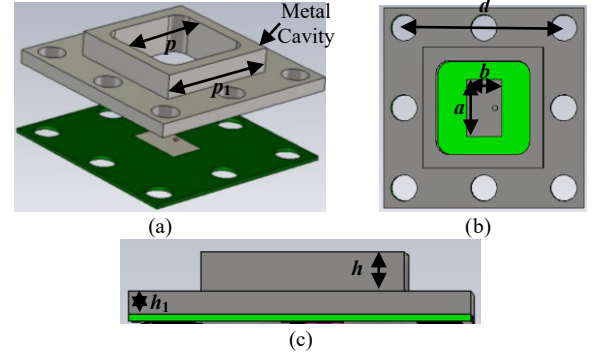

Fig. 2. The configurations of the feeding source. (a). Perspective view of the feeding antenna with a metal cavity. (b). Front view of the feeding antenna with a metal cavity. (c). Side view of the feeding antenna with a metal cavity.

A. Planar feeding source

Instead of using an open-ended waveguide as a feeding source, a planar patch antenna is adopted as it is expected to be integrated with the phase-shifting surfaces together, not adding an extra profile. Compared with the SIW slots and SIW aperture coupling antennas as the feeding sources for folded RA antennas [17], [20], a patch antenna can not only provide similar impedance bandwidth but also have a simple and easy method to adjust its impedance match. Fig. 2 shows the configurations of the planar patch antenna, where its total size is chosen as 15 mm × 15 mm × 0.305 mm. The dielectric substrate used is Rogers RO4003C with a thickness of 0.305 mm, a dielectric constant of 3.55, and a loss tangent of 0.0029.

For the conventional TA and RA antennas, EM waves radiate from the feeding source and then impinge on the phase-shifting surfaces directly to achieve a focused beam. However, EM waves from the feeding source of folded RA and TA antennas would be reflected by the polarizer firstly and then propagate through the phase-shifting surfaces to achieve a focused beam [20]-[23]. As shown in Fig. 3, it is better to regard the planar feeding source and the metal plate together as the exact source to illuminate the phase-shifting surfaces. Therefore, the radiation patterns of the exact source are investigated and presented. Fig. 4 (a) presents the 3-D radiation pattern (directivity) of the exact source at 28 GHz, where it is observed that the radiation pattern seems not uniform and symmetrical in E-plane (xoz) and H-plane (yoz). In order to improve the radiation patterns, a metal cavity is introduced to enclose the rectangular metal patch as shown in Fig. 2(a)-(b). Eight cylindrical holes with a radius of 1 mm are drilled to fix the metal cavity and substrate tightly. The metal cavity can

concentrate the EM field to make the radiation pattern of the patch antenna more uniform and symmetrical as shown in Fig. 4 (b). To achieve good performance of a RA or TA antenna, a feeding source with a radiation pattern shown in Fig. 4 (b) is preferred which will be verified in the subsequent subsection. The final dimensions of the planar feeding sources are listed as follows: a=4.3 mm, b=2.6 mm, p=7 mm, p_1=9 mm, h=1.8 mm, h_1=1.0 mm, d=12 mm, the feeding point is away from the center of the radiation patch 0.8 mm.
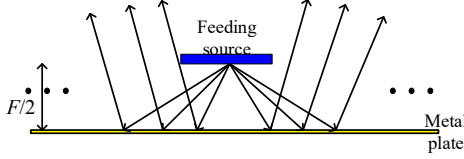

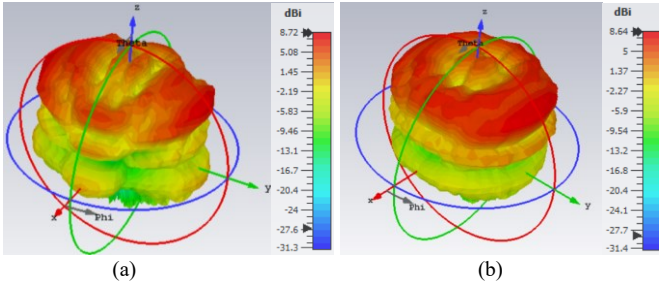Fig. 3. The configuration of the exact feeding source.

Fig. 4. The simulated 3-D radiation pattern (directivity) at 28 GHz for the exact feeding source [shown in Fig. 3]. (a). Without a metal cavity. (b). With a metal cavity.
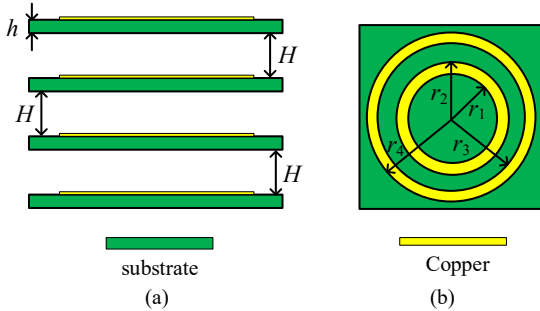

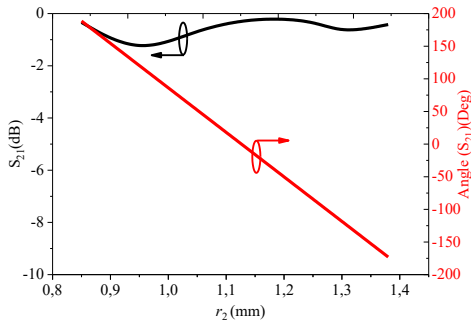Fig. 5. The configurations of the unit cell. (a). Side view. (b). Front view.

Fig. 6. The transmission phase and transmission amplitude of the unit cell with different values of r_2. (h = 0.305 mm, H = 2.5 mm, r_4 = 2.25 mm, r_3 = 1.75 mm, r_2 - r_1 = 0.5 mm)
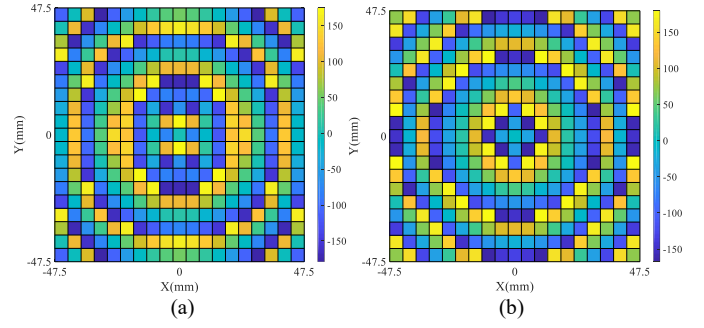

Fig. 7. The phase distributions on the same plane at 28 GHz (a). Feeding source without a metal cavity. (b). Feeding source with a metal cavity.
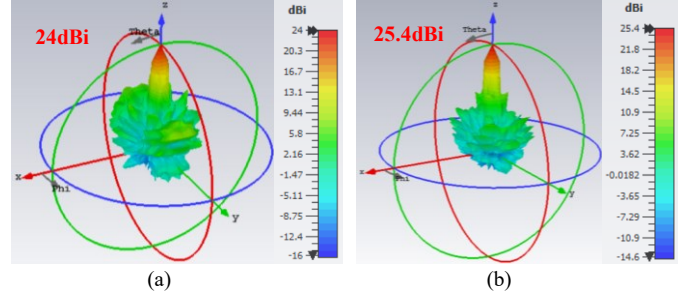

Fig. 8. The simulated 3-D radiation pattern (directivity) at 28 GHz of the proposed TA antenna. (a). Without a metal cavity. (b). With a metal cavity.

B. Implementation of the proposed low-profile TA antenna

Here, a four-layered double metal rings structure with an air separation of a quarter-wavelength is utilized as the unit cell for the constructions of the phase-shifting surfaces [24]-[26]. The configurations of the unit cell are shown in Fig. 5. The size of the unit cell is 5 mm * 5 mm. The substrates used here are also Rogers RO4003C with a thickness of 0.305mm. It is found that a full phase-cycle can be achieved by tuning either the radius of the inner or outer ring of the unit cell. As seen in Fig. 6, by varying radius and maintaining the width of the inner ring with other parameters fixed, a 2π transmission phase coverage at 28 GHz is obtained when the value of r_2 is varied from 0.85 to 1.40 mm. Besides, the transmission attenuation of the unit cell at 28 GHz is less than 1.2 dB within the entire phase-cycle coverage as can be checked in Fig. 6.

The proposed low-profile TA antenna is then performed according to the configuration shown in Fig.1, where the value of F and the size of the phase-shifting surface are 40 mm and 95 mm * 95 mm, respectively. In order to validate the performance enhancement caused by the planar feeding source with a metal cavity loaded, two TA antennas with the same profile are established, where one is illuminated by a feeding source with a metal cavity loaded, and the other one is illuminated by a feeding source without a metal cavity loaded. The phase distributions of the two TA antennas on the same plane are simulated and plotted at 28 GHz as shown in Fig. 7. According to the phase distributions, the corresponding TA antennas are established by using the unit cells shown in Fig.5. The directivities of the two TA antennas are simulated at 28 GHz. As seen in Fig. 8, the TA antenna illuminated by a feeding source with a metal cavity loaded can provide a higher directivity than

the one without a metal cavity loaded, which verify the effectiveness of introducing a metal cavity.

(a)   (b)
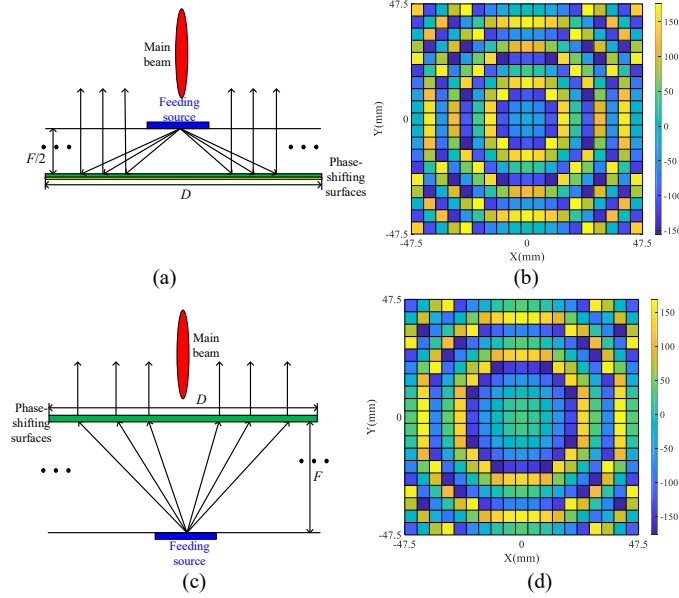

(c)   (d)

Fig. 9. (a). The schematic diagram of the RA antenna for reference. (b). The corresponding phase distributions. (c). The schematic diagram of the TA antenna for reference. (d). The corresponding phase distributions.
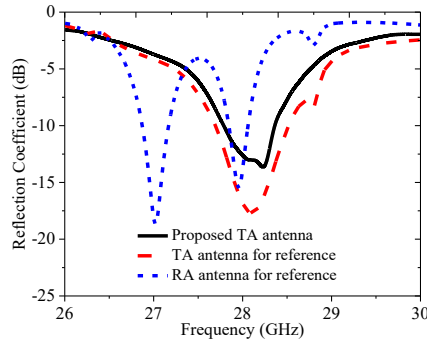

Fig. 10. The reflection coefficients of the three antennas.

C. Comparisons

Since the proposed TA antenna is implemented by the folding principles, a convincing comparison is needed between the proposed TA antenna and a conventional TA antenna whose profile is twice than that of the proposed TA antenna to evaluate their performance. Besides, we also compare the performance of the proposed TA antenna with a RA antenna whose profile is the same as the proposed TA antenna. The configurations of the RA and TA antennas for references are depicted in Fig. 9 (a) and (c). Similarly, the phase distributions on the prescribed planes for the RA and TA antennas for references are simulated and plotted in Fig. 9 (b) and (d), respectively. According to the phase distributions, the corresponding RA and TA antennas are established as well based on the unit cells shown in Fig. 5. The reflection coefficients and radiation patterns of these three antennas are simulated and compared. In order to obtain a fair and reasonable comparison, the dimensions of the feeding

sources should be the same and are allowed to be modified slightly to have good impedance match at 28 GHz. As seen in Fig. 10, the proposed TA antenna and the TA antenna for reference have very similar reflection coefficients, indicating an approximate 500 MHz impedance bandwidth. For the RA antenna for reference, there are two distinct resonances at 27 and 28 GHz in reflection coefficient. Noted that there should be a single resonance for the patch antenna-based feeding source. Since the phase-shifting surfaces are close to the feeding source, EM interferences happen on the plane of the phase-shifting surfaces of the RA antenna for reference, resulting in the reflection coefficient splitting into two distinct resonances as shown in Fig. 10. It is found that one of the two distinct resonances would become weaker and be disappeared finally when the phase-shifting surfaces are away from the feeding source. For a fair comparison, it is not allowed to significantly modify the feeding source or move the phase-shifting surface away from the feeding source to obtain a similar bandwidth than that of the proposed TA antenna and the TA antenna for reference. The simulated reflection coefficients indicate that the proposed TA antenna has a better impedance matching than that of the RA antenna for reference under the same conditions (the same ratio of focal-length-to-diameter, the same feeding source).
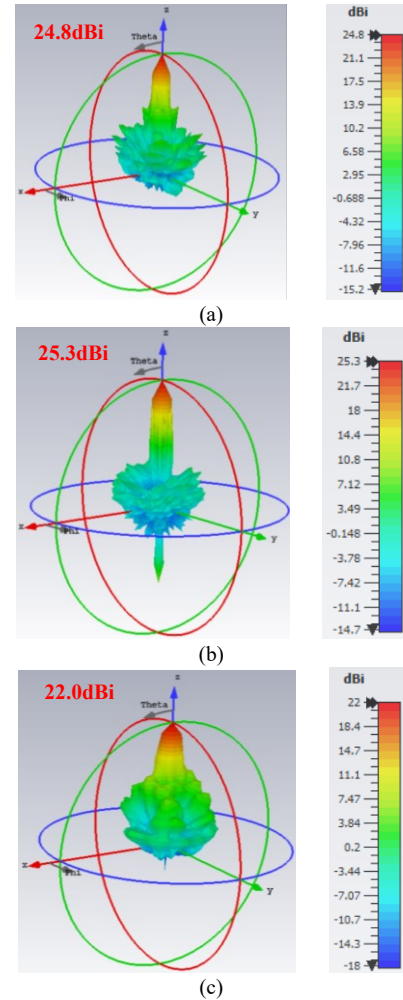

(a)

(b)

(c)

Fig. 11. The realized gains of the three antennas at 28 GHz. (a). The proposed low-profile TA antenna (24.8 dBi). (b). The TA antenna for reference (25.3 dBi). (c). The RA antenna for reference (22.0 dBi).
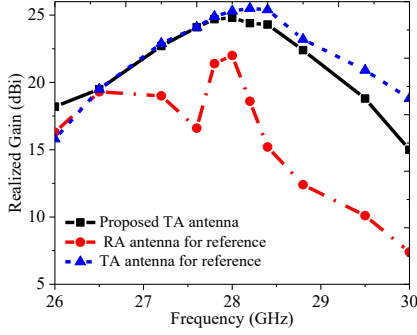

Fig. 12. The simulated realized gains of the proposed TA antenna, the RA antenna for reference, and the TA antenna for reference.

The realized gains of these three antennas are simulated and compared. Fig. 11 presents the 3-D radiation patterns of these three antennas at 28 GHz. It is observed that the RA antenna for reference has the smallest realized gain of 22.0 dBi; in contrast, the proposed TA antenna and the TA antenna for reference have similar realized gains of 24.8 dBi and 25.3 dBi, respectively. The realized gains of the three antennas from 26.0 to 30.0 GHz are also simulated and compared. As seen in Fig. 12, the realized gains of the RA antenna for reference are always lower than the other two antennas within the entire frequency band. The realized gains of the proposed TA antenna are slightly lower but very comparable to those of the TA antenna for reference within the entire frequency band. The realized gain discrepancies of the proposed TA antenna and the TA antenna for reference are attributed to the following reasons: a). The finite size of the metal plate used in the proposed TA antenna, where there exist some EM scatterings at the edges of the metal plate; b). For the proposed TA antenna, there is a blockage caused by the feeding source which does not exist in the TA antenna for reference.

Table I summarizes the three metrics (profile, realized gain, and aperture efficiency) of the three antennas. It is concluded that the proposed TA antenna has a lower profile, and comparable realized gain and aperture efficiency.

Table I. Performance comparison of the three antennas

Antenna Type	Frequency	Profile (mm, λ_0)	Realized Gain	Aperture Efficiency
RA antenna for reference	28 GHz	20, 1.87 λ_0	22.0 dBi	16 %
TA antenna for reference	28 GHz	40, 3.74 λ_0	25.3 dBi	34.3 %
Proposed TA antenna	**28 GHz**	**20, 1.87 λ_0**	**24.8 dBi**	**31.3 %**

III. LOW-PROFILE AND BEAM-STEERABLE TRANSMITARRAY ANTENNA

In this section, the proposed TA antenna in section II is expanded to achieve beam-steerable capabilities. In general, there are two passive methods to achieve beam-steerable TA

and RA antennas. One is mechanically moving the feeding source along a straight/arc trajectory or rotating the phase-shifting surfaces along a specific axis. The other one is employing multiple feeding sources, where each feeding source is responsible for a beam in a specified direction. Here, we adopt the second method to achieve beam steering since the feasibility, stability, and speed of mechanical control solution may be a problem in practice.
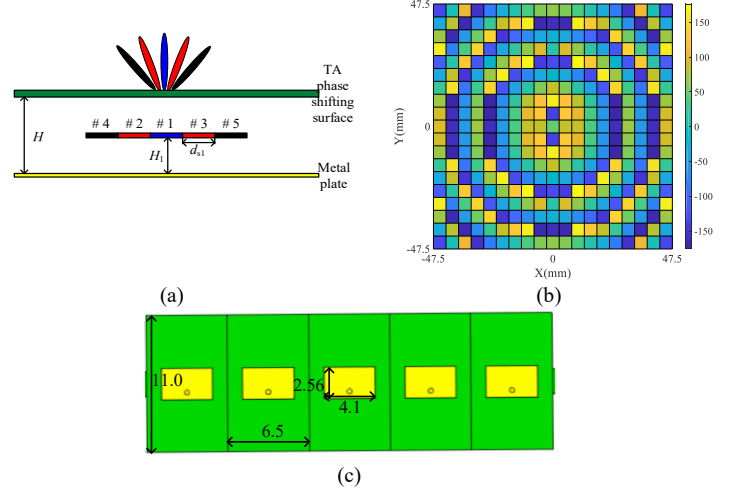

Fig. 13. (a). The configurations of the low-profile TA antenna with 5 feeding sources for five beams; (b). The phase distributions on the plane; (c). The dimensions of the five feeding sources (unit: mm)
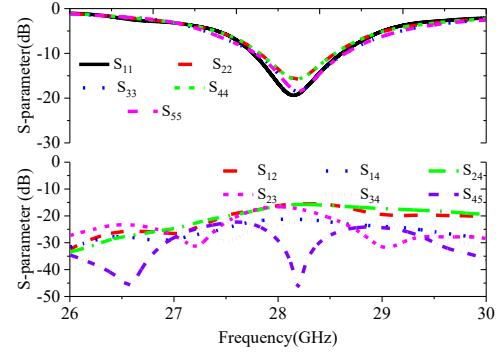

Fig. 14. The phase distributions on the TA aperture of the beam scanning antenna with 5 feeding sources.
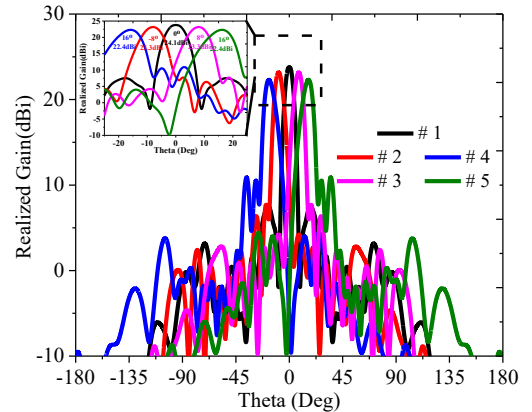
Fig. 15. The radiation patterns of the beam-steerable TA antenna with the feeding source #1, #2, #3, #4, and #5 excited at 28 GHz, respectively.

If the configuration in Fig. 1 is still applied for the beam-steerable TA antenna design, the multiple feeding sources integrated into the phase-shifting surfaces would occupy some unit cells. In order to keep complete of the phase-shifting surfaces, the multiple feeding sources can be located between the phase-shifting surfaces and metal plate as shown in Fig. 13 (a). In this configuration, the dimensions of the feeding source are optimized to minimize the blockage of the feeding source arrays as much as possible. On the other hand, the metal cavities are avoided due to their relatively big footprints. The dimensions and arrangements of the five feeding sources are shown in Fig. 13 (c). Here, the value of H is still 20 mm. The multiple feeding sources are separated from the metal plate with a separation of H_1 equal to 10 mm. The feeding point is away from the center of the radiation patch of 0.8 mm.

In order to obtain a symmetrically beam-steerable coverage, it is required that the multiple feeding sources should be distributed symmetrically, as illustrated in Fig. 13 (a). The feeding source # 1 is responsible for a focused beam at broadside. The feeding sources of # 2-5 are responsible for the main beams with different tilted angles off-broadside directions. Therefore, the phase-shifting surfaces are determined based on the phase distributions when port # 1 is excited. According to the phase distributions as plotted in Fig. 13(b), the corresponding TA antenna with beam steering is established. The S-parameters of the proposed antenna are simulated and shown in Figs. 14. All feeding sources have the impedance bandwidth of around 1.0 GHz with a port-to-port isolation of over 18 dB as shown in Fig. 14.

Fig. 15 presents the radiation patterns of the beam-steerable TA antenna at 28 GHz, where five beams are distributed symmetrically. The main beam at broadside has a realized gain of 24.1 dBi when port 1 is excited. The beam-steerable performance is obtained when the remaining ports are excited sequentially. Two beams are pointing toward ± 8º with the realized gain of 23.3 dBi, and two beams pointing toward ± 16º with the realized gain of 22.4 dBi. A gain variation of 1.7 dB is obtained within the entire beam-steerable coverage.

The beam-steerable resolution of the proposed beam-steerable TA antenna are also investigated based on a simplified schematic diagram shown in Fig. 16. Here, the beam-steerable resolution is defined by "the scanning angle difference of the adjacent feeding sources". The desired phases at U1 and U2 can be formulated based on the geometrical optics method for feeding sources of # 1 and # 2, respectively. After processing these phases, some methods to control beam-steerable resolution are drawn and summarized as follows:

a). the beam-steerable resolution would be increased when the value of s becomes bigger;

b). the beam-steerable resolution would be decreased when the value of l becomes bigger;

c). the beam-steerable resolution would be decreased when the value of dp becomes bigger;

In order to validate the effectiveness of the solutions, three cases with different l and s are simulated and their results are listed in Table. II, where only l and s are changed with the other parameters h and d_p fixed. The simulated results shown in Table. II are highly consistent with the aforementioned conclusions. It is observed that increasing the spacing of adjacent feeding sources and the numbers of the feeding sources are effective to increase the coverage of beam steering.
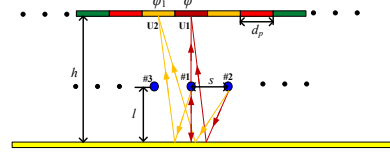

Fig. 16. The simplified schematic diagram for the beam-steerable TA antenna.

Table. II. Beam-steerable resolution under different values of l and s

	l	s	Beam-steerable resolution
Case 1	10 mm	6.5 mm	8º
Case 2	10 mm	8.5 mm	11º
Case 3	13 mm	6.5 mm	7º

IV. FABRICATION, MEASUREMENT, AND DISCUSSION

The proposed TA antenna, the RA and TA antennas for references, and the beam-steerable TA antenna have been fabricated and measured. All boards are produced with printed circuit board (PCB) technologies. There are 16 air holes with diameters of 3 mm uniformly distributed at the edges of every board. In order to support four-layered phase-shifting surfaces, some lightweight foams whose relative permittivity is approximately 1 with desired thicknesses are inserted between layers to support them and avoid any bendings of these boards. Metal plates are produced with mechanical mining technologies to be served as reflective surfaces for the proposed TA antennas. The separation between the feeding sources and phase-shifting surfaces is determined with some metal pillars with specific thicknesses.

Fig. 17 shows the photographs of the fabricated antennas. As seen in Fig. 17 (a), the proposed TA antenna and the RA antenna for reference have the same profiles and are half than that of the TA antenna for reference. Since the phase-shifting surfaces are implemented with a four-layered structure and the planar feeding source is co-planar with the first layer (that is most close to the metal plate), the MMPX connector can be hidden within the phase-shifting surfaces as shown in Fig. 17 (b), without adding extra profile for the proposed TA antenna. Fig. 17 (c) presents the front view of the beam-steerable TA antenna, where five feeding sources can be excited individually. The feeding sources are hidden between the phase-shifting surfaces and metal plate as shown in Fig. 17 (d), not adding extra profile for the beam-steerable TA antenna either.
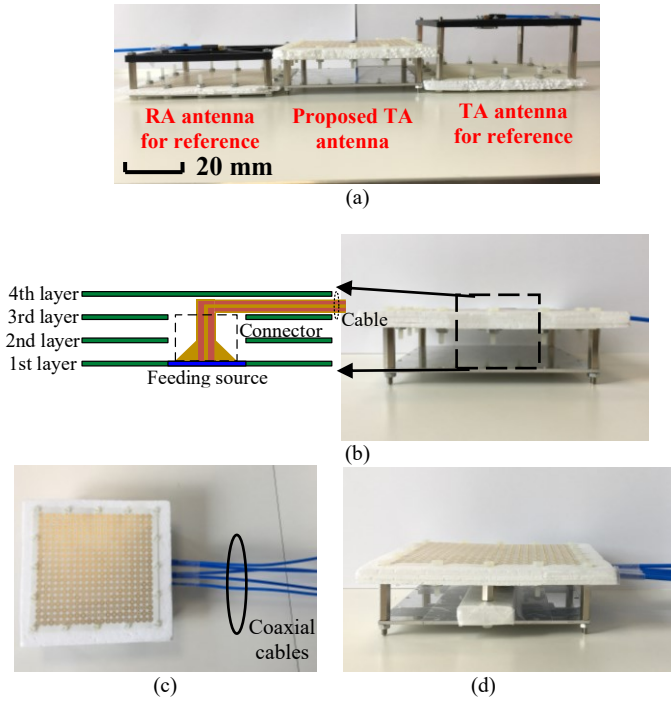
Fig. 17. The photographs of the proposed TA antenna, the RA antenna for reference, the TA antenna for reference, and the beam-steerable TA antenna with five beams. (a). Side view of the RA antenna for reference, the proposed TA antenna, and the TA antenna for reference. (b). Side view of the proposed TA antenna. (c). Front view of the beam-steerable TA antenna with five beams. (d). Side view of the beam-steerable TA antenna.

A. Reflection coefficients

The reflection coefficients of the proposed TA antenna, the RA antenna for reference, the TA antenna for reference, and the beam-steerable antenna are measured with the Keysight N5227A Power Network Analyzer (PNA) respectively as shown in Figs. 18 and 19, where it is observed that the measured reflection coefficients are all shifting toward lower frequencies more or less. The discrepancies are probably attributed to the permittivity of the substrates used in fabrications lower than the value in simulations.

B. Realized gain and radiation patterns

The realized gains of the proposed TA antenna, the RA antenna for reference, and the TA antenna for reference are measured. As seen in Fig. 20, the peak realized gains are all shifting toward lower frequencies that are highly consistent with the measured reflection coefficients. The measured peak gain of the proposed TA antenna is 24.3 dBi at 27.6 GHz; the corresponding aperture efficiency can be calculated by $\eta = G*\lambda^2/(4\pi S)$, where G is the realized gain, λ is the wavelength, and S is the physical area of the phase-shifting surfaces, resulting in an aperture efficiency of 28 %. Tab. III compares the simulated and measured realized gains and aperture efficiency of the proposed TA antenna. In contrast, the peak gain of the TA antenna for reference is 25.1 dBi at 27.2 GHz; and the peak gain of the RA antenna for reference is 21.8 dBi at 26.2 GHz. Compared with the simulated realized gains shown in Fig. 12, the measured results are reasonable except for the frequency shifting. From Fig. 20, it is observed that the realized

gains of the proposed TA antenna are higher than the counterparts of the RA antenna for reference; on the other hand, the proposed TA antenna has the similar realized gain with the TA antenna for reference, which verifies the effectiveness of the proposed TA antenna sufficiently.
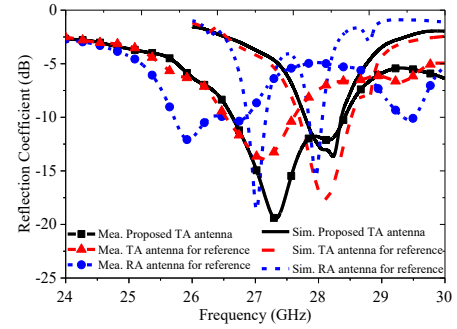

Fig. 18. Measured and simulated reflection coefficients of the RA antenna for reference, the proposed TA antenna, and the TA antenna for reference.
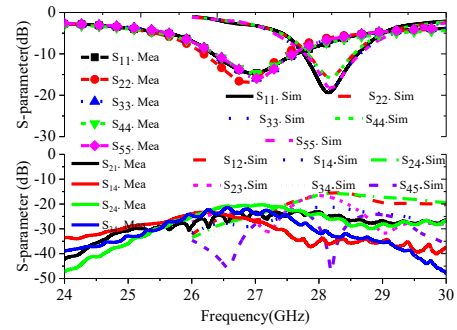

Fig. 19. Measured and simulated S-parameter of the beam-steerable TA antenna.
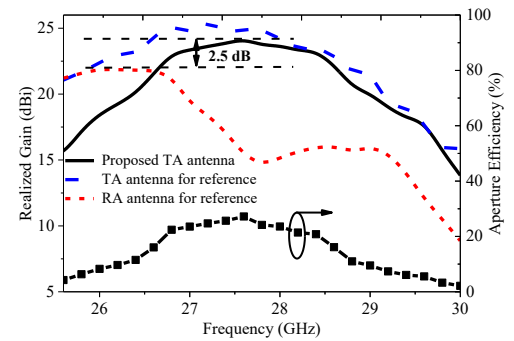
Fig. 20. Measured realized gains of the proposed TA antenna, the RA antenna for reference, and the TA antenna for reference; the measured aperture efficiency of the proposed TA antenna.

Table. III. Simulated and measured results comparisons for the proposed TA antenna.

	Frequency	Realized Gain	Aperture Efficiency
Simulated	28.0 GHz	24.8 dBi	31.3 %
Measured	27.6 GHz	24.3 dBi	28 %

The normalized radiation patterns of the proposed TA antenna are measured and compared with the simulated results. As seen in Fig. 21, the measured and simulated co-polarizations (co-pol) in E- and H-plane are highly consistent. The sidelobe levels of

the proposed TA antenna in E- and H-plane are all better than -20 dB. The normalized cross-polarizations (cro-pol) in E-plane and H-plane are all below - 20 dB.

It is found that the beam-steerable TA antenna has a peak realized gain at 27.2 GHz, which is consistent with the measured reflection coefficient. Therefore, the radiation patterns of the beam-steerable TA antenna are measured at 27.2 GHz. During the measurements, the remaining ports are all matched to perfect loads when one port is excited. As seen in Fig. 22, the main beam is pointing toward broadside when port 1 is excited. Its realized gain reaches 24.0 dBi, resulting in an aperture efficiency of 27 %. In contrast, when port 2 or 3 is excited individually, the main beam is pointing toward -8° or +8° off-broadside with a realized gain of 23.0 dBi or 23.2 dBi, respectively; and the main beam is fixed at -16° or +16° off-broadside when port 4 or 5 is excited individually, with a realized gain of 21.2 dBi or 21.6 dBi, respectively. The measured beam pointing directions are highly consistent with the counterparts of the simulated results, except for minor gain drops.

for the main beam at broadside. A peak aperture efficiency of 27.0% is obtained at 27.2 GHz with a realized gain of 24.0 dBi. As seen in Fig. 23, the maximum gain variation of the beam-steerable TA antenna is around 5.0 dB within the entire beam-steerable coverage from 26 to 28 GHz. The gain variation over the frequency band can be improved by using wideband unit cells to implement the phase-shifting surfaces since the wideband unit cell can provide low attenuations in a wide bandwidth, or optimizing the phase-shifting surfaces by using bifocal phase distribution or other phase distributions [27]-[29].

In order to compare the proposed beam-steerable TA antenna with a similar and state-of-the-art RA and TA antennas, a table regarding some important figures of merits is made and summarized in Tab. IV, where it can be concluded that the proposed beam-steerable TA antenna has a lower profile, satisfactory aperture efficiency, simple design procedures, and is feasible for dual-polarized applications.

Fig. 22. The measured gains of the beam-steerable TA antenna with five beams at 27.2 GHz.
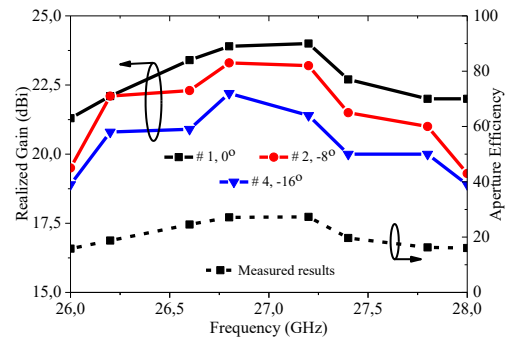
Fig. 23. The measured realized gain of the beam-steerable TA antenna with five beams when port 1, 2, and 3 are excited individually; and the aperture efficiency of the beam-steerable TA antenna with five beams when only port 1 is excited.
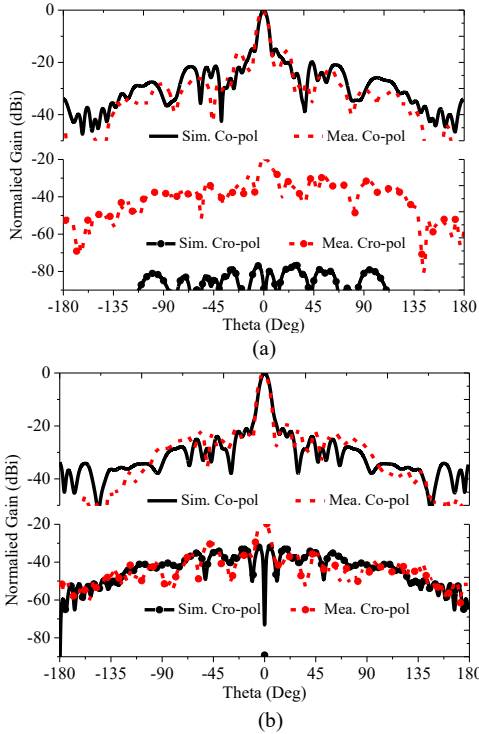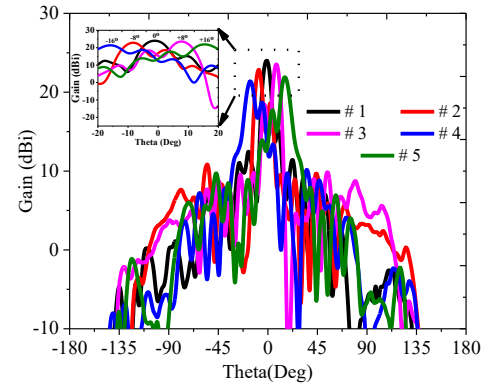

Fig. 21. Measured and simulated normalized radiation patterns of the proposed TA antenna. (a). E-plane. (b). H-plane (Due to the frequencies shifting for the measured results, the measured radiation patterns at 27.6 GHz and the simulated radiation patterns at 28.0 GHz are compared)

Fig. 23 presents the realized gains of the beam-steerable TA antenna from 26 to 28 GHz when port 1, 2, and 4 is excited individually with the remaining ports well matched. It is observed that the realized gains of the beam-steerable TA antenna are highest when port 1 is excited. In contrast, the realized gains become lower when the main beam is pointing toward 8 and 16 deg off-broadside direction. The aperture efficiency of the beam-steerable TA antenna is also calculated

Table. IV. Performance comparisons of the proposed beam-steerable TA antenna with the existing similar TA and RA antennas.

Ref	[15] TAP 2017	[16] TAP 2018	[17] MTT 2018	[18] TAP 2018	This work
Frequency (GHz)	27.5	42	40.25	26	**27.2**
Thickness mm, λ_0	54mm 4.95 λ_0	25mm 3.50 λ_0	24mm 3.22 λ_0	81mm 7.02 λ_0	**20mm 1.84 λ_0**

Realized gain (dBi)	24.2	25.9	27.4	24.8	**24.0**
Pol.*	Dual	Single	Single	Dual	**Dual**
Beam-steerable technique	Multiple feeding sources	Multiple feeding sources	Rotating P-S surfaces	Multiple feeding sources	**Multiple feeding sources**
Comp.#	Simple	Moderate	Moderate	Simple	**Simple**
Num.	7	7	7	9	**5**
Gain variation/ Beam coverage	3.7dB/ (-27°, +27°)	2.0dB/ (-10°, +10°)	N.AdB/ (-7°, +7°)	3.0dB/ (-40°, +40°)	**2.4dB/ (-16°, +16°)**
Aperture efficiency	24.5 %	11.0 %	27.3 %	4.0 %	**27.0 %**

*Pol.: polarization; #: simple means only phase-shifting surfaces should be synthesized, moderate means a polarization rotation surface should be considered as well except for the phase-shifting surfaces; NA: not mentioned and can't be deduced from the manuscript either.

V. Conclusion

In conclusion, a beam-steerable and low-profile TA antenna has been proposed in this paper. In the proposed design, a metal plate is used to replace a polarizer in the existing folded TA and RA antennas to simplify the design procedures and make the proposed antenna feasible for dual-polarized applications. In order to demonstrate to superiorities of the proposed antenna, a RA antenna for reference and a TA antenna for reference are also simulated, measured, and compared. It is concluded that the proposed TA antenna has a higher gain and a lower profile. The proposed TA antenna is expanded to achieve beam steering by employing multiple feeding sources. A beam-steerable TA antenna with five beams has been fabricated and measured. The measured results reveal that the beam-steerable TA antenna can realize $\pm$ 16°, $\pm$ 8°, 0° beam pointing directions with a gain variation of 2.4 dB within the entire coverage of 32°. The peak aperture efficiency of the beam-steerable TA antenna is 27 % for the main beam at broadside. Due to the low-profile and beam-steerable properties, the proposed beam-steerable TA antenna is a good candidate for 5G millimeter-wave communications.

Acknowledgements

References

[1] T. Pappaport, *et al.*, "Millimeter wave mobile communication for 5G cellular: it will work!" *IEEE Access*, vol. 1, pp. 335-349, May 2013.

[2] W. Hong, *et al.*, "Multibeam antenna technologies for 5G wireless communications," *IEEE Trans. Antennas Propag.*, vol. 65, no. 12, pp. 6213-6231, Dec 2017.

[3] A. Miura, S. Yamamoto, H. Li, M. Tanaka, and H. Wakana, "Ka-band aeronautical satellite communications experiments using COMEFS," *IEEE Trans. Veh. Technol.*, vol. 55, no. 5, pp. 1153-1164, Sep 2002.

[4] G. Han, B. Du, W. Wu, and B. Yang, "A novel hybrid phased array antenna for satellite communication on-the-move in Ku-band," *IEEE Trans. Antennas Propag.*, vol. 63, no. 4, pp. 1375-1383, Apr 2015.

[5] A. Jacomb-Hood, and E. Lier, "Multibeam active phased arrays for communications satellites," *IEEE Microw. Mag.*, vol. 1, no. 4, pp. 40-47, Dec 2000.

[6] G. Kant, P. Patel, S. Wijnholds, M. Ruiter, and E. van der Wal, "EMBRACE: A multi-beam 20,000-element radio astronomical phased array antenna demonstrator," *IEEE Trans. Antennas Propag.*, vol. 59, no. 6, pp. 1990-2003, Jun 2011.

[7] D. Kang, K. Koh, and G. Rebeiz, "A Ku-band two-antenna four-simultaneous beams SiGe BiCMOS phased array receiver," *IEEE Trans. Microw. Theory Techn.*, vol. 58, no. 4, pp. 771-780, Apr 2010.

[8] M. Sayginer, and G. Rebeiz, "An eight-element 2-16 GHz programmable phased array receiver with one, two, or four simultaneous beams in SiGe BiCMOS," *IEEE Trans. Microw. Theory Techn.*, vol. 64, no. 12, pp. 4585-4597, Dec 2016.

[9] E. Lier, D. Purdy, and K. Maalouf, "Study of deployed and modular active phased-array multibeam satellite antenna," *IEEE Antennas Propag. Mag.*, vol. 45, no. 5, pp. 34-45, Oct. 2003.

[10] E. Lier, and R. Melcher, "A modular and lightweight multibeam active phased receiving array for satellite applications: Design and ground testing," *IEEE Antennas Propag. Mag.*, vol. 51, no. 1, pp. 80-90, Feb. 2009.

[11] C. Huang, W. Pan, X. Ma, B. Zhao, J. Cui, and X. Luo, "Using reconfigurable transmitarray to achieve beam-steering and polarization manipulation applications," *IEEE Trans. Antennas Propag.*, vol. 63, no. 11, pp. 4801-4810, Nov. 2015.

[12] J. Lau, and S. Hum, "A wideband reconfigurable transmitarray element," *IEEE Trans. Antennas Propag.*, vol. 60, no. 3, pp. 1303-1311, Mar. 2012.

[13] P. Padilla, A. Munoz-Acevedo, M. Sierra-Castaner, and M. Sierra-Perez, "Electronically reconfigurable transmitarray at Ku band for microwave applications," *IEEE Trans. Antennas Propag.*, vol. 58, no. 8, pp. 2571-2579, Aug. 2010.

[14] J. Lau, and S. Hum, "Reconfigurable transmitarray design approaches for beamforming applications," *IEEE Trans. Antennas Propag.*, vol. 60, no. 12, pp. 5679-5689, Dec. 2012.

[15] M. Jiang, Z. Chen, Y. Zhang, W. Hong, and X. Xuan, "Metamaterial-based thin planar lens antenna for spatial beamforming and multibeam massive MIMO," *IEEE Trans. Antennas Propag.*, vol. 65, no. 2, pp. 464-472, Feb. 2017.

[16] Y. Hu, W. Hong, and Z. Jiang, "A multibeam folded reflectarray antenna with wide coverage and integrated primary sources for millimeter-wave massive applications," *IEEE Trans. Antennas Propag.*, vol. 66, no. 12, pp. 6875-6882, Dec. 2018.

[17] J. Yang, Y. Shen, L. Wang, H. Meng, W. Dou, and S. Hu, "2-D scannable 40-GHz folded reflectarray fed by SIW slot antenna in a single-layered PCB," *IEEE Trans. Microw. Theory Techn.*, vol. 66, no. 6, pp. 3129-3135, Jun. 2018.

[18] Y. Hu, W. Hong, C. Yu, Y. Yu, H. Zhang, Z. Yu, and N. Zhang, "A digital multibeam array with wide scanning angle and enhanced beam gain for millimeter-wave massive MIMO applications," *IEEE Trans. Antennas Propag.*, vol. 66, no. 11, pp. 5827-5837, Nov. 2018.

[19] G. Liu, M. Kodnoeih, K. Pham, E. Cruz, D. Gonzalez-Ovejero, and R. Sauleau, "A millimeter-wave multibeam transparent transmitarray antenna at Ka-band," *IEEE Antennas Wireless Propag. Lett.*, vol. 18, no. 4, pp. 631-635, Apr. 2019.

[20] M. Jiang, W. Hong, Y. Zhang, S. Yu, and H. Zhou, "A folded reflectarray antenna with a planar SIW slot array antenna as the primary source," *IEEE Trans. Antennas Propag.*, vol. 62, no. 7, pp. 3575-3583, Jul. 2014.

[21] D. Pilz, and W. Menzel, "Printed mm-wave folded reflector antennas with high gain, low loss, low profile," in Proc. *IEEE Int. Symp. Antennas Propag.,* vol. 2, pp. 790-793, Jun. 2000.

[22] Y. Ge, C. Lin, and Y. Liu, "Broadband folded transmitarray antenna based on an ultrathin transmission polarizer," *IEEE Trans. Antennas Propag.*, vol. 66, no. 11, pp. 5974-5981, Nov. 2014.

[23] C. Fan, W. Che, W. Yang, and S. He, "A novel PRAMC-based ultralow-profile transmitarray antenna by using ray tracing principle," *IEEE Trans. Antennas Propag.*, vol. 65, no. 4, pp. 1779-1787, Apr. 2017.

[24] A. Abdelrahman, A. Elsherbeni, and F. Yang, "Transmission phase limit of multilayer frequency selective surfaces for transmitarray designs," *IEEE Trans. Antennas Propag.*, vol. 62, no.2, pp. 690-697, Feb. 2014.

[25] P. Mei, S. Zhang, and G. F. Pedersen, "A dual-polarized and high-gain X/Ka-band shared-aperture antenna with high aperture reuse efficiency", submitted to *IEEE Trans. Antennas Propag.*

[26] A. Abdelrahman, A. Elsherbeni, and F. Yang, "Transmitarray antenna design using cross-slot elements with no dielectric substrate," *IEEE Antennas Wireless Propag. Lett.,* vol. 13, pp. 177-180, 2013.

[27] P. Nayeri, F. Yang, and A. Z. Elsherbeni, "Bifocal design and aperture phase optimizations of reflectarray antenna for wide-angle beam scanning performance," *IEEE Trans. Antennas Propag.*, vol. 61, no. 9, pp. 4588-4597, Sep. 2013.

[28] P. Nayeri, F. Yang, and A. Z. Elsherbeni*, Reflectarray Antennas: Theory. Designs, and Applications*, Wiley-IEEE Press, Feb. 2018.

[29] P. Nayeri, F. Yang, and A. Z. Elsherbeni, "Planar reflectarray antennas with spherical phase distribution for two-dimensional beam-scanning," *2013 US National Committee of URSI National Radio Science Meeting (USNC-URSI NRSM),* Boulder, CO, pp. 1-1, 2013.